ChemPhysChem

Research Article
doi.org/10.1002/cphc.202401043

Chemistry Europe
European Chemical Societies Publishing

www.chemphyschem.org

Competition Between Halogen Atom and Ring of Halobenzenes as Hydrogen Bond Electron Donor Sites

Akhtam Amonov[a] and Steve Scheiner*[b]

A halobenzene molecule contains several sites that are capable of acting in an electron-donating capacity within a H–bond. One set of such sites comprise the lone electron pairs of the halogen (X) atoms on the periphery of the ring. The π-electron system above the ring plane can also fulfill this function in many cases. DFT calculations are applied to compare and contrast the propensity of these two site types to engage in such a H–bond within the context of mono, di, tri, tetra, and hexasubstituted halobenzenes. The X atoms chosen for study comprise the full set: F, Cl, Br, and I. It is found that even when the electrostatic potential of the X lone pair is more negative than that above the ring, it is the latter position which is the preferred binding site of HCl in most cases. This preference switches over to the X lone pair only for higher order of substitution, with n = 4 or 6. This pattern is explained in large measure by the higher contribution of dispersion when the proton donor is located above the ring.

Introduction

The interactions between molecules are of paramount importance in nearly all aspects of chemistry and biology, arguably as important as the much stronger covalent bonding that holds the atoms together within each molecule. The hydrogen bond (HB) is the most prevalent and important of all noncovalent interactions, and figures prominently in a wide range of phenomena such as solvation, genetic replication, and enzymatic activity[1–10].

The HB is commonly summarized in the context of AH··B where A and B refer to the proton donor and acceptor, respectively. A major component of the bonding is the partial transfer of some charge from B to AH, so A and B are also frequently respectively referred to as electron acceptor and donor units. The specific source of the electron density that is being transferred from B is often a lone electron pair. But there are alternate sources as well, such as the electrons within a bonding π-orbital of an alkene or alkyne, for example. The latter idea can be expanded within the framework of an extended conjugated system such as butadiene. The highly delocalized and flexible π-cloud of an aromatic system offers another opportunity for electron donation within a HB. Indeed, such AH··π bonding is frequently invoked to help understand the structure and function of a multitude of systems.[11–21]

A halogenated aromatic ring furnishes two very interesting and competing options. On one hand, the halogen (X) atom, whether F, Cl, Br, or I, contains several lone pairs which can readily serve as electron donor sites. And the partial negative charge on the X atom ought to augment the electrostatic component of the HB, through its direct interaction with the positive H. But also, the aromatic π-cloud of the ring offers an alternative source of charge which could potentially be transferred to the proton donor unit. And this same π-cloud provides a negative region of electrostatic potential, directly above and below the plane of the ring.

This pair of dual possibilities raises the immediate question as to which bonding mode will be preferred. In order to address this question by quantum chemical means, a series of substituted benzenes was considered. Either 1, 2, 3, 4, or 6 halogen atoms are added to a benzene ring, with X covering the full range of F, Cl, Br, and I halogens. For each substituted benzene, a HCl molecule was allowed to approach and form each of the two sorts of HBs, either to the X atom or to the π-system above the ring. The energetics of each was assessed, and then the results analyzed as to the underlying reasons for the preference of one mode of H-bonding or the other. One idea considered is whether the relative stabilities of the two sorts of HBs are directly related to the numerical value of the electrostatic potential at the two sites. Another issue concerns how well AIM mimics of HB strength reproduce the actual energetics.

Methods

The Gaussian 16[22] suite of programs was employed to carry out the quantum chemical calculations, applying the DFT M06-2X functional[23] in conjunction with the triple-ζ def2-TZVP basis set. The pseudopotential placed on I by this basis takes into consideration certain relativistic effects. M06–2X has been repeatedly assessed to be one of the most accurate functionals for H-bonding and related noncovalent interactions[24–32]. Geometries were fully optimized, and characterized as true minima

[a] Dr. A. Amonov
Department of Optics and Spectroscopy, Engineering Physics Institute, Samarkand State University, University blv. 15, Samarkand 140104, Uzbekistan

[b] Prof. S. Scheiner
Department of Chemistry and Biochemistry, Utah State University, Logan, Utah 84322-0300, USA
E-mail: steve.scheiner@usu.edu

Supporting information for this article is available on the WWW under https://doi.org/10.1002/cphc.202401043

by harmonic vibrational analysis which yielded all positive frequencies. The interaction energy E_{int} is equal to the difference between the energy of the dyad and the sum of the energies of the two monomers in the geometry they adopt within the complex; E_{int} was corrected for basis set superposition error by the standard counterpoise prescription.[33]

The Multiwfn program[34] located and quantified the minima of the molecular electrostatic potential (MEP) on the $\rho = 0.001$ au isodensity surface of each isolated monomer. Atoms in Molecules (AIM) bond paths and the properties of their associated critical points were evaluated via the AIMAll program.[35] Total interaction energies were decomposed into their contributing components by Symmetry-Adapted Perturbation Theory (SAPT)[36,37] at the SAPT0 level through the PSI4 program.[38]

Results

The X atoms were placed on the benzene ring as follows. When $n = 2$, the two X atoms were placed opposite one another in a *para* arrangement. Three X atoms occupied 1,3,5 positions, again maximizing their distance apart. 1,2,4,5 positions were taken for $n = 4$, and all six sites were of course taken for $n = 6$. Two different bonding arrangements were found when each such ring was approached by a HCl molecule. A standard HB was formed when HCl approached one of the X atoms of the ring, with a nearly linear ClH··X alignment. The other stable geometry located the HCl above the phenyl ring, with the H pointing down toward the approximate center of the ring, in what is termed a π-geometry.

Geometries

The most important aspects of the intermolecular geometries are highlighted in Figure 1, using the dibrominated benzene for illustrative purposes. For the case when the HCl is involved in a ClH··X HB to one of the X atoms, R is defined as the H··X distance. The α angle indicates the linearity of this HB, and the CX··H angle is defined as β. The other class of interactions places the HCl above the benzene plane. The distance from the H to the center of the benzene ring is defined as R, and the angle made by the ClH molecule and the center of the ring is α.

The details of the geometry for the various dyads are displayed in Tables 1 and 2 for the X and π geometries respectively, and there are several trends that are apparent. The HB distances in Table 1 elongate as the X atom grows larger, for any value of *n*. This trend is sensible in light of the enlarging X radius. As more X atoms are added to the ring, the HB distance grows longer. This pattern is consistent with the idea that the added electron-withdrawing X atoms pull density away from each other, making each a weaker nucleophile. (This notion is confirmed by the analyses of the monomer electrostatic potentials below.)

An α angle of 180° corresponds to perfect linearity within the HB. These angles all deviate from linearity by varying amounts. In fact, some of these deviations are quite large, with α as small as 102°. With regard to the placement of the bridging proton in relation to the X atom, β angles in the neighborhood of 90–120° are consistent with the locations of the X lone pairs. The β angles in Table 1 span a wide range from 48° to 123°, largest for F. The last parameter included in Table 1 is the φ(HXCC) dihedral angle which quantifies how far out of the phenyl plane the H atom is located. The very small values, mainly for the fluorosubstituted rings, place the H near the ring plane, while it is located far above this plane for dihedral angles approaching 90°.

With regard to the π geometries, the distance between the H and the ring center, defined as R, is fairly uniform from one system to the next, hovering between 2.30 and 2.38 Å for the most part. This distance is a bit longer for the tetrasubstituted rings, regardless of the nature of X. And importantly, there are no minima on the potential energy surface for any of the hexasubstituted rings, as explained in more detail below. The α angle in Figure 1b relates again to the linearity of the HB, but in this case involves the center of the ring rather than an X atom. There is a certain degree of "tilt" in many cases, as α differs from 180° for most of the dyads, with the exception of $n = 3$, for which HCl is nearly perpendicular to the ring. The greatest

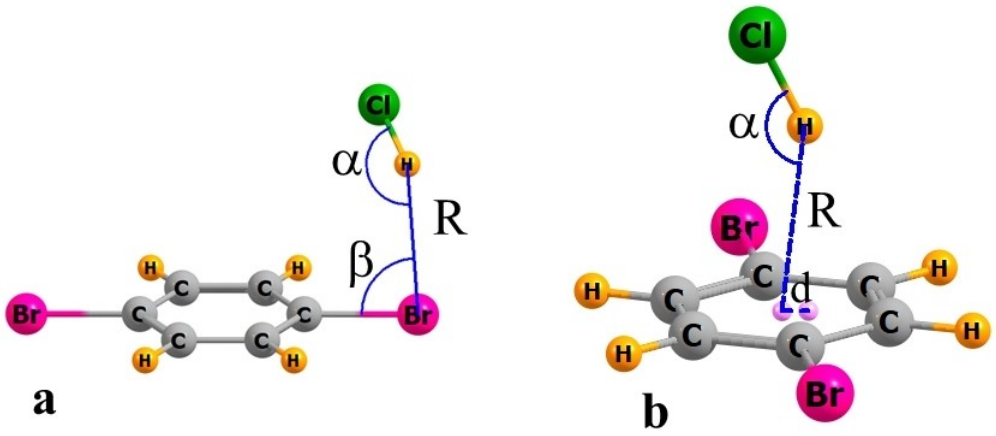

Figure 1. Geometrical parameters defined for a) X and b) π configurations of HCl paired with p-dibromobenzene

Table 1. Geometrical aspects of X geometries (Å and degs).

	R	α	β	φ(HXCC)
n = 1				
F	2.089	156.3	112.3	44.9
Cl	2.586	153.5	77.4	89.4
Br	2.678	161.2	74.0	99.3
I	2.830	161.5	87.8	33.9
n = 2				
F	2.120	154.6	123.2	0.0
Cl	2.636	146.0	78.0	89.2
Br	2.657	157.6	85.6	50.0
I	2.879	168.9	98.1	90.2
n = 3				
F	2.161	152.6	122.7	12.6
Cl	2.668	147.2	76.2	89.2
Br	2.719	152.1	82.2	56.5
I	2.939	147.3	80.8	51.2
n = 4				
F	2.210	145.6	122.1	19.4
Cl	2.838	120.5	55.5	61.0
Br	2.756	147.8	47.8	60.1
I	2.949	147.7	48.0	60.0
n = 6				
F	2.847	101.9	70.0	48.5
Cl	2.936	124.5	58.7	62.9
Br	2.949	136.0	64.2	72.8
I	3.234	135.9	56.4	72.0

Table 2. Geometrical aspects of π geometries (Å and degs)

	R	α	d
n = 1			
F	2.349	154.8	0.39
Cl	2.339	152.3	0.25
Br	2.349	150.9	0.28
I	2.308	170.1	0.08
n = 2			
F	2.373	148.3	0.29
Cl	2.381	146.3	0.31
Br	2.377	146.7	0.32
I	2.370	146.8	0.28
n = 3			
F	2.351	161.8	0.14
Cl	2.323	179.2	0.00
Br	2.322	179.3	0.01
I	2.311	179.5	0.00
n = 4			
F	2.587	122.5	0.43
Cl	2.577	121.7	0.44
Br	2.517	126.2	0.45
I	2.476	129.2	0.44

deviation approaching a nearly horizontal, almost parallel alignment, occurs for $n = 4$, with α angles between 122° and 129°. The last parameter included in Table 2 is d which refers to the displacement of HCl atom from the center of the ring. More precisely, d is the distance between the ring center and the projection of the H atom into the ring plane, both indicated by pink spheres in Figure 1b. For $n = 3$, this displacement is quite small, which coincides with the values of α near 180°. However, for the other dyads, d is considerably larger, particularly those for $n = 4$ where d exceeds 0.4 Å. So not only is the HCl molecule tilted away from the perpendicular, with α angles substantially less than 180°, but the H lies some distance from the ring center.

Some of these structures are shown explicitly in Figure 2 to add further context, with the coordinates of all dyads provided in the Supplementary Information.

Energetics and Electrostatic Potentials

The energetics of the various complexes are contained in the first three columns of Table 3. The first two values correspond to the counterpoise-corrected interaction energies of each. These quantities are generally between 2 and 3 kcal/mol. There is an overall pattern for these energies as they slowly diminish as n rises, consistent with the bond lengthening mentioned above. As far as the particular X substituent goes, there is little differentiation between F, Cl, Br, and I. The specific pattern as to the relationship between n and X is not straightforward. For example, Cl engages in the strongest X geometry for $n = 4$ but it is I that takes this mantle for $n = 3$ or $n = 6$. There is a bit more regularity in the π structures in that X≡I forms the strongest complexes, particularly for the larger values of n.

A central issue relates to the competition between the X and π sites. For most systems, it is the π structure which is the more strongly bound. The advantage of π over X is listed in the next column of Table 3. This advantage is largest for n = 1 at 1 kcal/mol, but generally diminishes for higher degrees of substitution. In fact, for the tetrasusbstituted F and Cl dyads, it is the X geometry which is favored. And of course, the balance completely shifts to the X structure for $n = 6$ as there are no stable π dyads. But by and large, the two different configurations are competitive in terms of interaction energy.

The strength of the binding ought to bear a relationship to the electrostatic potential to which the HCl is drawn. One means of quantifying this attractive power is via V_{min}, defined here as the minimum of the molecular electrostatic potential (MEP) on the 0.001 au isodensity surface. These quantities are listed in the next columns of Table 3. The X minimum is located roughly along a X lone pair direction while that situated above the benzene plane is labeled π. The values of these V_{min} are most negative for the singly substituted benzene, between −11 and −17 kcal/mol. The absolute value of this quantity drops

Research Article
doi.org/10.1002/cphc.202401043
Chemistry Europe
European Chemical Societies Publishing

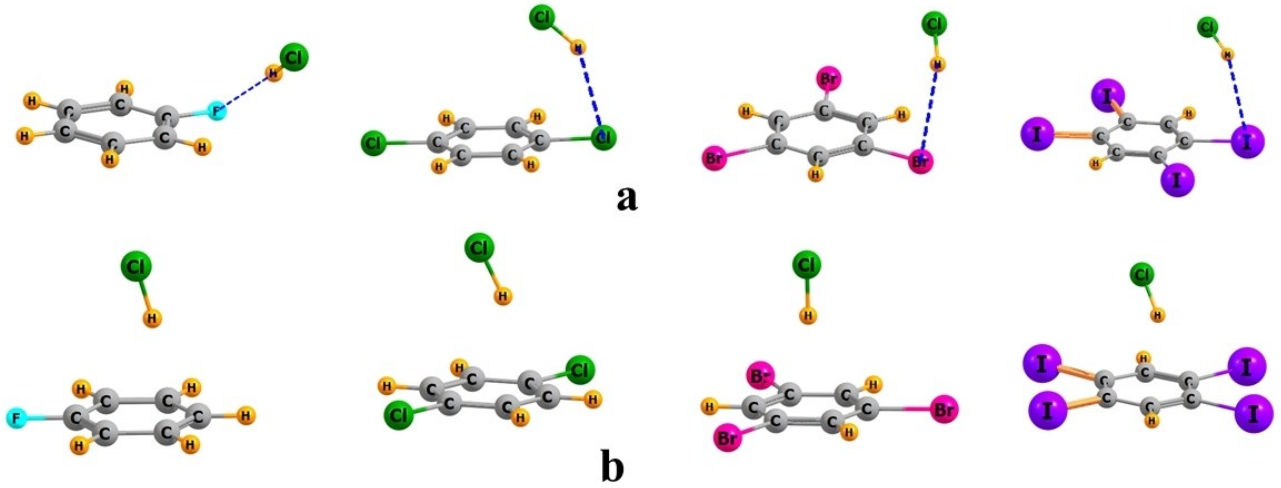

Figure 2. Optimized geometries in selected dyads of HCl in a) X and b) π structures.

Table 3. Interaction energies of complexes with HCl, MEP minima of optimized monomers of halogenated benzene (kcal/mol), and bond critical point densities (au) of relevant bonds in dyads.

	$-E_{int}$			V_{min}			ρ_{BCP}		
	X	π	π-X	X	π	π-X	X	π	π-X
n = 1									
F	2.56	3.42	1.00	−16.8	−12.0	4.8	0.0148	0.0102	-0.0046
Cl	2.51	3.35	0.95	−12.6	−10.9	1.7	0.0108	0.0091	-0.0017
Br	2.62	3.28	0.78	−12.4	−10.4	2.0	0.0112	0.0091	-0.0021
I	2.54	3.37	1.02	−11.3	−10.6	0.7	0.0114	0.0083	-0.0031
n = 2									
F	2.48	2.59	0.21	−14.2	−5.6	8.6	0.0136	0.0089	-0.0047
Cl	2.31	2.65	0.50	−9.0	−4.7	4.3	0.0099	0.0090	-0.0009
Br	2.46	2.63	0.29	−8.7	−4.2	4.5	0.0120	0.0091	-0.0029
I	1.68	2.80	1.39	−7.9	−5.1	2.8	0.0102	0.0088	-0.0014
n = 3									
F	2.03	2.03	0.16	−10.0	−0.4	9.6	0.0124	0.0088	-0.0036
Cl	2.09	2.26	0.53	−5.8	−0.1	5.7	0.0093	0.0230[a]	0.0137
Br	2.18	2.31	0.17	−5.7	−0.5	5.2	0.0106	0.0230[a]	0.0104
I	2.24	2.57	0.46	−5.6	−1.0	4.6	0.0093	0.0233[a]	0.0140
n = 4									
F	2.00	1.58	-0.30	−12.7	+4.7	17.4	0.0113	0.0073	-0.0040
Cl	2.59	2.07	-0.46	−9.5	+3.3	12.8	0.0131[a]	0.0073	-0.0058
Br	2.22	2.17	0.15	−8.7	+3.2	11.9	0.0100	0.0082	-0.0018
I	2.35	2.53	0.42	−7.7	+0.7	8.4	0.0090	0.0086	-0.0004
n = 6									
F	1.97	x	x	−5.9	+15.8	21.7	[b]	x	x
Cl	2.62	x	x	−5.9	+9.3	15.2	0.0120[a]	x	x
Br	2.85	x	x	−6.3	+7.5	13.8	0.0071	x	x
I	3.00	x	x	-6.8	+2.8	9.6	[b]	x	x

[a] sum of multiple bond paths [b] paths do not involve H

along with the X electronegativity: F > Cl > Br > I for both the X and π minima. As more X substituents are added to the ring, V_{min} becomes progressively less negative, and even positive when *n* exceeds 3. It might be noted as well that there is a

small enhancement of the X lump between $n=3$ and 4. This is attributed to the partial coalescence of the lumps of adjacent X atoms for $n=4$.

In all cases, V_{min} is more negative near the X atom as compared to what might be termed the "π-lump" above the ring, This advantage, reported in the π-X column of Table 3, is largest for F, and drops as the X atom grows larger. Another important trend is the growth of the X advantage as n increases. Although less than 5 kcal/mol for $n=1$, the π-X advantage rises to the 10–22 kcal/mol range for $n=6$.

Some of the finer points concerning these MEP minima arise in the context of their precise positioning. The small green spheres in Figure 3 labeled as X identify their positions for the halogenated benzenes. It may be noted first that the π minima do not lie precisely above the ring center. Taking $n=1$ as an example, this minimum lies closer to the C atom opposite or *para* to the Br substituent. The other X minimum lies above the plane of the molecule, with an angle θ defining its precise position. Whereas Figure 3a pertains specifically to bromobenzene, the other related monohalogenated benzenes have very similar V_{min} dispositions. As is evident in Figure 3b, adding a second X atom places the π minima nearly above the C–C bonds of the C atoms that are unsubstituted. This same theme continues for $n=3$ and 4, as Figure 3c and 3d show the minima lie above the unsubstituted C atoms. Figure 3d illustrates the aforementioned coalescence of the X lumps between each pair of adjacent X atoms to a single lump for $n=4$.

Unlike the smaller values of n, the MEP for $n=6$ has a somewhat different shape for each X substituent. In the first place, the π-lumps lie above the C–C bonds for F, Cl, and I, whereas they are situated directly above the six C atoms for Br. Regarding the lumps involving the X lone pairs, each F atom contains its own pair of minima, for a total of 12. On the other hand, the coalescence of these pairs for Cl or I to a single lump reduces this number to 6, that are each midway between a pair of Cl/I atoms. The number of minima is also 6 for Br, but these points are situated closer to Br atoms than to their midpoints.

The positioning of the HCl molecule is only partially connected to the locations of the minima in the MEP of the ring. With respect to the X configurations, the MEP minima around the X atom are located well above the ring plane for $n<4$, which matches pretty well with the HCl position. However, there are exceptions for $n=2$ and 3 for F, where HCl lies within the aromatic plane. The discrepancy between V_{min} and HCl locations is more obvious for larger values of n. For example, even though V_{min} for F_4 lies between each pair of adjacent F atoms, HCl occupies a site between a F and H atom. Also, HCl points toward one Br atom of Br_4, not toward a midpoint between two Br atoms. There are similar disconnects between V_{min} and HCl for a number of π configurations. Taking $n=1$ as a case in point, as indicated in Figure 3a, V_{min} sits above the C atom *para* to the X substituent. While the ClH axis points toward this *para* C for F and Cl, verified by an AIM bond axis, it is a *meta* C to which the H of ClH is bonded for Br, which switches again to an *ortho* C for I.

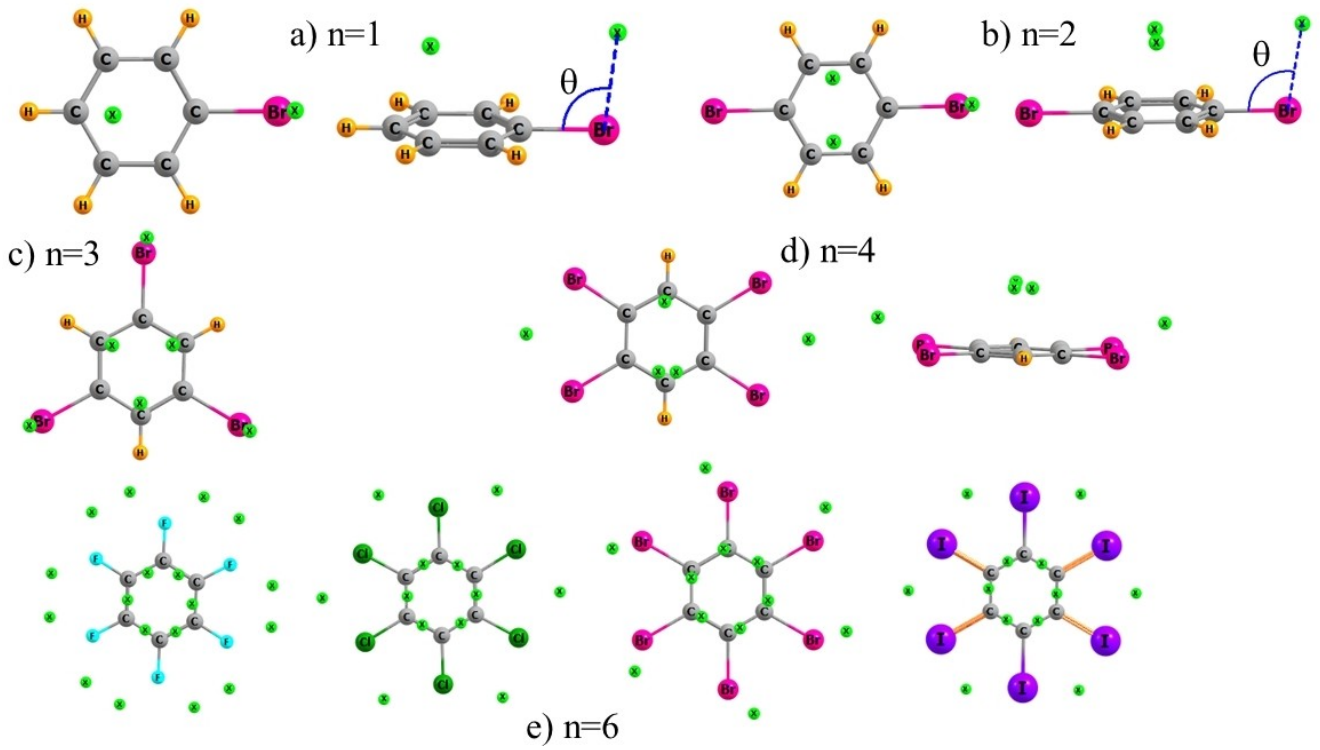

Figure 3. Positions of minima in the MEP of halogenated benzenes, shown as small green spheres labeled with an X.

Composition of Interaction Energies

Clearly then, while the location of V_{min} has some influence over HCl positioning, it is not necessarily the dominant factor. And as indicated above, the relative energies of the X and π geometries do not necessarily follow the same trend as the magnitudes of their MEPs. So it would appear that Coulombic forces may not dominate the interactions. In an effort to scrutinize the influence of electrostatics, the total interaction energy of a number of complexes was decomposed by SAPT into its constituents. The electrostatic term (ES) is attractive for each complex listed in Table 4 for $n=1$ and $n=4$ which is opposed by the exchange repulsion (EX). Also contributing to the attraction are the induction (IND) and dispersion (DISP) energies.

It is immediately apparent that ES is not the dominant attractive element. While ES contributes about half of the total attraction for the X configuration for F, it is much smaller for the others. With the exception of the latter configuration, ES accounts for only between 18% and 41% of this total. Induction plays an even lesser role, less than 20% in most cases. The largest contributor is dispersion whose percentage can be as large as 67%. The share that is attributable to dispersion is larger for the π configurations as compared to the X structures, and is larger for $n=4$ than for the monosubstituted benzenes.

Comparison of the numerical values of each contributor offers a glimpse into the underlying reason for the overall preference of the π over the X geometries which can conflict with V_{min} predictors. Taking as an example the I_1 data set in Table 4, ES favors X over π by 0.35 kcal/mol. EX and IND largely cancel one another. It is the 1.60 kcal/mol DISP difference that makes the difference in favor of π, reversing the trend predicted by ES. Indeed, this pattern is characteristic of most of the data in Table 4. While ES generally favors X over π with positive entries for π-X, the large negative quantities for DISP are the primary factor in shifting the balance toward π. The exceptions noted above are F_4 and Cl_4, where the DISP push toward π is overshadowed by the combined pull toward X by ES and EX.

So overall, dispersion plays a larger role in the stability of most of these complexes. Its influence can outweigh that of electrostatics, so must be considered not only in terms of relative energetics, but also in guiding the establishment of the most stable geometries of each. For example, a nonlinearity of the HB, as exemplified by smaller α angles, has the advantage of bringing the Cl atom, with its 17 electrons, in closer toward the aromatic ring, which would amplify the dispersive interaction.

Table 4. SAPT decomposition of interaction energy (kcal/mol) for complexes with HCl.

n=1		ES	EX	IND	DISP	% ES	%IND	%DISP
F	X	−4.09	4.77	−1.15	−2.42	53.4	15.0	31.7
	π	−3.42	5.55	−1.70	−4.30	36.3	18.1	45.6
	π-X	0.67	0.78	−0.56	−1.88			
Cl	X	−2.55	4.72	−1.23	−3.63	34.4	16.6	49.0
	π	−3.20	5.52	−1.56	−4.59	34.2	16.7	49.1
	π-X	−0.65	0.80	−0.33	−0.95			
Br	X	−2.65	4.76	−1.39	−3.58	34.8	18.2	47.0
	π	−3.09	5.47	−1.53	−4.63	33.4	16.6	50.1
	π-X	−0.44	0.71	−0.14	−1.05			
I	X	−3.33	5.42	−1.82	−2.95	41.1	22.5	36.4
	π	−2.99	5.08	−1.47	−4.55	33.2	16.3	50.5
	π-X	0.35	-0.33	0.35	−1.60			
n=4								
F	X	−3.29	3.84	−0.84	−2.07	53.1	13.6	33.3
	π	−1.51	5.25	−1.06	−4.26	22.1	15.5	62.4
	π-X	1.77	1.40	−0.22	−2.20			
Cl	X	−2.51	5.13	−0.83	−4.44	32.2	10.7	57.1
	π	−1.64	5.37	−1.04	−5.22	20.7	13.2	66.1
	π-X	0.87	0.24	−0.21	−0.78			
Br	X	−2.81	5.33	−1.15	−3.88	35.8	14.7	49.5
	π	−1.62	5.53	−1.12	−5.60	19.4	13.4	67.2
	π-X	1.19	0.20	0.04	−1.72			
I	X	−2.50	5.47	−1.36	−4.21	31.0	16.8	52.2
	π	−1.68	5.78	−1.36	−6.08	18.4	14.9	66.7
	π-X	0.82	0.31	0.00	-1.87			

Analysis of the topology of the electron density in these complexes amplifies on some of the trends described above. The last three columns of Table 3 include the density at the relevant AIM bond critical points between H of HCl and the relevant atom of the halobenzene. In most cases, this density is larger for the X configuration than for the π-geometry, again despite the lesser stability of the former. It is likely that the higher interaction energies for the π-complexes are due in large measure to their higher proportional contribution of dispersion which is poorly accounted for by AIM. The exceptions to this trend arise in connection with several of the trisubstituted π complexes where the symmetrical location of the H leads to three bond paths leading from this center to C atoms of the ring. One factor helping to stabilize the X structure from the standpoint of AIM is the presence of a second bond path that connects the Cl of HCl with one of the phenyl H atoms, consistent with the idea of a weak CH··Cl HB in several of these systems. Although the density of this path is quite low, it would tend to augment the ClH··X HB, so the fact that the X geometry remains less stable than π is further evidence of the important influence of dispersion.

Conclusions

The benzene ring contains an area of negative potential both above and below that is capable of attracting the positive end of a HCl molecule. When coupled with the availability of the its π-electron cloud, benzene can thus act as electron donor in a ClH··π HB. Replacing one or more H atoms of benzene with halogen atoms draws a certain amount of density away from this π-lump above the ring, reducing its availability and making the potential less negative. The ensuing bond weakening increases as more and more such halosubstitutions are made, to the point that the hexahalogenated benzene can no longer form such a HB.

The halogen atom on a benzene ring can itself act as electron donor in a HB to HCl through its lone pairs and accompanying negative potential. Even though V_{min} on the X atom of monohalogenated benzene is more negative than the π-lump above the ring, it is the ClH··π HB above the ring that is stronger than the more conventional ClH··X HB to the X lone pair. This apparent contradiction rests on the greater contribution of dispersion to the ClH··π bond than to ClH··X, which preferentially stabilizes the former.

Further halosubstitution continues to withdraw electron density from each X atom, just as it does from the π-lump above the ring, reducing the magnitude of V_{min} on X, an effect that grows progressively with each additional halosubstitution. Each such X addition has a greater effect on the π-lump than on X. It is not until 4 or more X atoms have been added that the ClH··X HB finally becomes stronger than the ClH··π interaction. This switch requires that V_{min} on X be more negative than the π-lump by 12 kcal/mol.

Acknowledgements

This material is based upon work supported by the National Science Foundation under Grant No. 1954310.

Conflict of Interests

The authors declare no conflict of interest.

Data Availability Statement

The data that support the findings of this study are available from the corresponding author upon reasonable request.

Keywords: Dispersion · Molecular electrostatic potential · Energy decomposition · Substituent effect

[1] G. C. Pimentel, A. L. McClellan, The Hydrogen Bond, Freeman, San Francisco, **1960**.
[2] S. N. Vinogradov, R. H. Linnell, Hydrogen Bonding, Van Nostrand-Reinhold, New York, **1971**.
[3] S. Scheiner, D. A. Kleier, W. N. Lipscomb, *Proc. Nat. Acad. Sci., USA.* **1975**, *72*, 2606–2610.
[4] M. D. Joesten, L. J. Schaad, Hydrogen Bonding, Marcel Dekker, New York, **1974**.
[5] M. M. Szczesniak, S. Scheiner, Y. Bouteiller, *J. Chem. Phys.* **1984**, *81*, 5024–5030.
[6] K. Luth, S. Scheiner, *J. Phys. Chem.* **1994**, *98*, 3582–3587.
[7] S. J. Grabowski in Hydrogen Bonding - New Insights, Vol. (Ed. Eds.: Editor), Springer, City, **2006**.
[8] A. Chand, D. K. Sahoo, A. Rana, S. Jena, H. S. Biswal, *Acc. Chem. Res.* **2020**, *53*, 1580–1592.
[9] M. Cuma, S. Scheiner, T. Kar, *J. Mol. Struct. (Theochem).* **1999**, *467*, 37–49.
[10] H. S. Biswal, S. Wategaonkar, *J. Chem. Phys.* **2011**, *135*, 134306.
[11] S. J. Grabowski, F. Ruipérez, *ChemPhysChem.* **2017**, *18*, 2409–2417.
[12] P. Mastrorilli, V. Gallo, S. Todisco, M. Latronico, G. Saielli, *Chem. Eur. J.* **2016**, *22*, 7964–7969.
[13] X. Zhang, H. Dai, H. Yan, W. Zou, D. Cremer, *J. Am. Chem. Soc.* **2016**, *138*, 4334–4337.
[14] K. L. Hudson, G. J. Bartlett, R. C. Diehl, J. Agirre, T. Gallagher, L. L. Kiessling, D. N. Woolfson, *J. Am. Chem. Soc.* **2015**, *137*, 15152–15160.
[15] M. Mirzaei, M. Nikpour, A. Bauzá, A. Frontera, *ChemPhysChem.* **2015**, *16*, 2260–2266.
[16] M. A. Trachsel, P. Ottiger, H.-M. Frey, C. Pfaffen, A. Bihlmeier, W. Klopper, S. Leutwyler, *J. Phys. Chem. B.* **2015**, *119*, 7778–7790.
[17] A. E. Aliev, J. R. T. Arendorf, I. Pavlakos, R. B. Moreno, M. J. Porter, H. S. Rzepa, W. B. Motherwell, *Angew. Chem. Int. Ed.* **2015**, *54*, 551–555.
[18] S. Ahnen, A.-S. Hehn, K. D. Vogiatzis, M. A. Trachsel, S. Leutwyler, W. Klopper, *Chem. Phys.* **2014**, *441*, 17–22.
[19] M. Nishio, Y. Umezawa, J. Fantini, M. S. Weiss, P. Chakrabarti, *Phys. Chem. Chem. Phys.* **2014**, *16*, 12648–12683.
[20] O. Takahashi, Y. Kohno, K. Saito, *Chem. Phys. Lett.* **2013**, *378*, 509–515.
[21] H. K. Ganguly, B. Majumder, S. Chattopadhyay, P. Chakrabarti, G. Basu, *J. Am. Chem. Soc.* **2012**, *134*, 4661–4669.
[22] M. J. Frisch, G. W. Trucks, H. B. Schlegel, G. E. Scuseria, M. A. Robb, J. R. Cheeseman, G. Scalmani, V. Barone, G. A. Petersson, H. Nakatsuji, X. Li, M. Caricato, A. V. Marenich, J. Bloino, B. G. Janesko, R. Gomperts, B. Mennucci, H. P. Hratchian, J. V. Ortiz, A. F. Izmaylov, J. L. Sonnenberg, D. Williams-Young, F. Ding, F. Lipparini, F. Egidi, J. Goings, B. Peng, A. Petrone, T. Henderson, D. Ranasinghe, V. G. Zakrzewski, J. Gao, N. Rega, G. Zheng, W. Liang, M. Hada, M. Ehara, K. Toyota, R. Fukuda, J. Hasegawa, M. Ishida, T. Nakajima, Y. Honda, O. Kitao, H. Nakai, T. Vreven, K. Throssell, J. A. Montgomery, J. E. Peralta, F. Ogliaro, M. J. Bearpark, J. J. Heyd, E. N. Brothers, K. N. Kudin, V. N. Staroverov, T. A. Keith, R. Kobayashi, J. Normand, K. Raghavachari, A. P. Rendell, J. C. Burant, S. S. Iyengar, J. Tomasi, M. Cossi, J. M. Millam, M. Klene, C.

Adamo, R. Cammi, J. W. Ochterski, R. L. Martin, K. Morokuma, O. Farkas, J. B. Foresman, D. J. Fox, Gaussian 16 Rev. C.01, Wallingford, CT, **2016**.
[23] Y. Zhao, D. G. Truhlar, *Theor. Chem. Acc.* **2008**, *120*, 215–241.
[24] G. Paytakov, T. Dinadayalane, J. Leszczynski, *J. Phys. Chem. A.* **2015**, *119*, 1190–1200.
[25] B. S. D. R. Vamhindi, A. Karton, *Chem. Phys.* **2017**, *493*, 12–19.
[26] R. Podeszwa, K. Szalewicz, *J. Chem. Phys.* **2012**, *136*, 161102.
[27] S. Karthikeyan, V. Ramanathan, B. K. Mishra, *J. Phys. Chem. A.* **2013**, *117*, 6687–6694.
[28] M. Majumder, B. K. Mishra, N. Sathyamurthy, *Chem. Phys.* **2013**, *557*, 59–65.
[29] M. A. Vincent, I. H. Hillier, *Phys. Chem. Chem. Phys.* **2011**, *13*, 4388–4392.
[30] A. D. Boese, *ChemPhysChem.* **2015**, *16*, 978–985.
[31] M. Walker, A. J. A. Harvey, A. Sen, C. E. H. Dessent, *J. Phys. Chem. A.* **2013**, *117*, 12590–12600.
[32] L. F. Molnar, X. He, B. Wang, K. M. Merz, *J. Chem. Phys.* **2009**, *131*, 065102.
[33] S. F. Boys, F. Bernardi, *Mol. Phys.* **1970**, *19*, 553–566.
[34] T. Lu, F. Chen, *J. Comput. Chem.* **2012**, *33*, 580–592.
[35] T. A. Keith, AIMAll, TK Gristmill Software, Overland Park KS, **2013**.
[36] K. Szalewicz, B. Jeziorski in *Symmetry-adapted perturbation theory of intermolecular interactions, Vol.* (Ed. S. Scheiner), Wiley, New York, **1997**, pp.3–43.
[37] R. Moszynski, P. E. S. Wormer, B. Jeziorski, A. van der Avoird, *J. Chem. Phys.* **1995**, *103*, 8058–8074.
[38] D. G. A. Smith, L. A. Burns, A. C. Simmonett, R. M. Parrish, M. C. Schieber, R. Galvelis, P. Kraus, H. Kruse, R. D. Remigio, A. Alenaizan, A. M. James, S. Lehtola, J. P. Misiewicz, M. Scheurer, R. A. Shaw, J. B. Schriber, Y. Xie, Z. L. Glick, D. A. Sirianni, J. S. O'Brien, J. M. Waldrop, A. Kumar, E. G. Hohenstein, B. P. Pritchard, B. R. Brooks, H. F. SchaeferIII, A. Y. Sokolov, K. Patkowski, A. E. DePrince III, U. Bozkaya, R. A. King, F. A. Evangelista, J. M. Turney, T. D. Crawford, C. D. Sherrill, *J. Chem. Phys.* **2020**, *152*, 184108.

Manuscript received: November 13, 2024
Revised manuscript received: January 25, 2025
Accepted manuscript online: January 27, 2025
Version of record online: February 5, 2025